Available online at www.sciencedirect.com
SCIENCE DIRECT®
International Journal of Solids and Structures 42 (2005) 2601–2623
INTERNATIONAL JOURNAL OF SOLIDS and STRUCTURES
www.elsevier.com/locate/ijsolstr

Two circular inclusions with inhomogeneously imperfect interfaces in plane elasticity

Xu Wang *, Junqian Zhang, Xingming Guo

Shanghai Institute of Applied Mathematics and Mechanics, Shanghai University, Yanchang Road, Shanghai 200072, PR China

Received 15 June 2004; received in revised form 1 October 2004
Available online 23 November 2004

Abstract

This paper is concerned with the problem of two circular inclusions with circumferentially inhomogeneously imperfect interfaces embedded in an infinite matrix in plane elastostatics. Infinite series form solutions to this problem are derived by applying complex variable techniques. The numerical results demonstrate that the interface imperfection, interface inhomogeneity, and interaction among neighboring inclusions (fibers) will exert a significant influence on the stresses along the interfaces and average stresses within the inclusions.

Keywords: Two circular inclusions; Imperfect interface; Complex variable techniques

1. Introduction

Theoretical work on composite materials with imperfect interfaces is emerging rapidly in recent years. Here the model of an imperfect interface is based on the premise that tractions are continuous but displacements are discontinuous across the interface. Furthermore, displacement jumps are proportional, in terms of the 'spring-factor-type' interface parameters, to their respective traction components. Most of the studies on this research topic were limited to constant interface parameter (see, for example, Achenbach and Zhu, 1990; Gulrajani and Mukherjee, 1993; Zhong and Meguid, 1997; Kattis and Providas, 1998; Pan et al., 1998; Tong et al., 2001; Mogilevskaya and Crouch, 2002, 2004). The variable interface parameter, which can be employed to reflect the more realistic scenario in which the extent of bonding at the interface varies

* Corresponding author. Tel./fax: +86 021 56338301.
E-mail address: xuwang@staff.shu.edu.cn (X. Wang).

0020-7683/$ - see front matter © 2004 Elsevier Ltd. All rights reserved.
doi:10.1016/j.ijsolstr.2004.10.002

along the interface, has recently evoked interest among researchers in this field (see, for example, Ru and Schiavone, 1997; Sudak et al., 1999; Chen, 2001; Wang and Shen, 2002).

This paper can be considered as a continuation of the work of Wang and Shen (2002) for anti-plane shear elasticity. In that paper, the authors considered two circular inclusions with circumferentially inhomogeneous imperfect interfaces interacting with a circular Eshelby inclusion in anti-plane shear. Their results indicate that interface imperfection, interface inhomogeneity, and interaction between the two closely spaced inclusions will exert a significant influence on the stress field within each of the two inclusions. The counterpart problem in plane elasticity is of more practical importance, and also more challenging. Kouris (1993) considered two circular inclusions with homogeneously sliding interfaces in plane elasticity based on Papkovich–Neuber displacement formulation. He observed that both the relative distance between the inclusions and the condition of the interface have a significant effect on the stress concentration. However, the problem of two circular inclusions with circumferentially inhomogeneous imperfect interfaces in plane elastostatics is still to be investigated.

In this research, we consider plane deformations of two circular inclusions with circumferentially inhomogeneous imperfect interfaces embedded in an infinite matrix. The interfaces adopted in this research can be characterized by those in which there is a displacement jump across the interface in the same direction as the corresponding tractions, and the same degree of imperfection is realized in both the normal and tangential directions. The two inclusions may possess distinct material properties and be of different sizes. Complex variable techniques are used to obtain infinite series form solutions for this problem. The numerical results demonstrate quantitatively how the interfacial stresses along the interfaces, and average stresses within each inclusion are influenced by the interface imperfection, interface inhomogeneity, and interaction between the two inclusions.

2. Basic formulation

Consider a domain in $\Re^2$, infinite in extent, containing two circular elastic inclusions as shown in Fig. 1. Let S_1, S_2 and S_3 denote the right inclusion, the matrix and the left inclusion, respectively. The center of the left

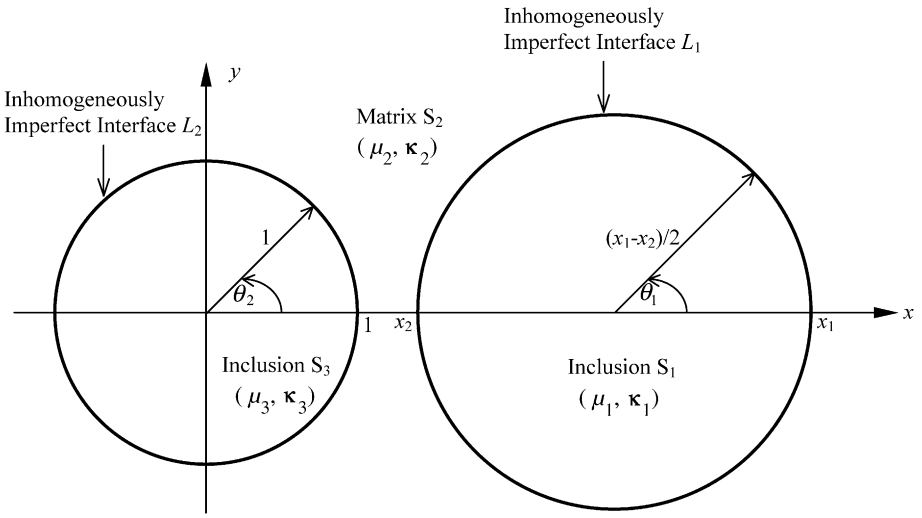

Fig. 1. Two circular inclusions with circumferentially inhomogeneous imperfect interfaces embedded in an infinite elastic matrix in plane elastostatics.

circular inclusion is at the origin of the Cartesian coordinate system, and the center of the right circular inclusion is on the x-axis. The left circular inclusion of radius 1 has elastic properties κ_3 and μ_3, the right circular inclusion of radius $(x_1 - x_2)/2$ has elastic properties κ_1 and μ_1, the matrix has elastic properties κ_2 and μ_2. The distance between the centers of the two inclusions is $(x_1 + x_2)/2$. Throughout this paper, the subscripts 1, 2, 3 (or the superscripts (1), (2) and (3)) are used to identify the respective quantities in S_1, S_2 and S_3.

For plane deformation, the stresses can be expressed in terms of the two Muskhelishvili's complex potentials $\phi(\zeta)$ and $\psi(\zeta)$ as (Muskhelishvili, 1953)

$$\begin{aligned}
&\sigma_{xx} + \sigma_{yy} = 4\mathrm{Re}\left[\frac{\phi'(\zeta)}{m'(\zeta)}\right],\\
&\sigma_{yy} - \sigma_{xx} + 2\mathrm{i}\sigma_{xy} = 2\frac{\overline{m(\zeta)}\left\{\frac{\phi'(\zeta)}{m'(\zeta)}\right\}' + \psi'(\zeta)}{m'(\zeta)},\\
&\sigma_{rr} + \sigma_{\theta\theta} = \sigma_{xx} + \sigma_{yy},\\
&\sigma_{\theta\theta} - \sigma_{rr} + 2\mathrm{i}\sigma_{r\theta} = \frac{\zeta^2 m'(\zeta)}{|\zeta|^2\overline{m'(\zeta)}}(\sigma_{yy} - \sigma_{xx} + 2\mathrm{i}\sigma_{xy}).
\end{aligned} \tag{1}$$

The displacements and resultant force can be expressed in terms of $\phi(\zeta)$ and $\psi(\zeta)$ as

$$F_x + \mathrm{i}F_y = (-\mathrm{i})\left[\phi(\zeta) + \frac{m(\zeta)}{\overline{m'(\zeta)}}\overline{\phi'(\zeta)} + \overline{\psi(\zeta)}\right], \tag{2}$$

$$2\mu(u_r + \mathrm{i}u_\theta) = \frac{|\zeta m'(\zeta)|}{\zeta m'(\zeta)}\left[\kappa\phi(\zeta) - \frac{m(\zeta)}{\overline{m'(\zeta)}}\overline{\phi'(\zeta)} - \overline{\psi(\zeta)}\right], \tag{3}$$

where $\kappa = 3 - 4\nu$ for plane strain (assumed henceforth in this research) and $\kappa = (3 - \nu)/(1 + \nu)$ for plane stress, and μ, ν are the shear modulus and Poisson's ratio, respectively. u_r and u_θ are the normal and tangential displacement components in the curvilinear coordinate system expressed by $m(\zeta)$.

The following conformal mapping function is considered (Cao, 1988)

$$z = m(\zeta) = \frac{\zeta - a}{a\zeta - 1}, \tag{4}$$

where

$$a = \frac{1 + x_1x_2 + \sqrt{(x_1^2 - 1)(x_2^2 - 1)}}{x_1 + x_2}. \tag{5}$$

As illustrated in Fig. 2, the above mapping function $m(\zeta)$ can map the two circular interfaces L_1, formed by the right inclusion and the matrix, and L_2, formed by the left inclusion and the matrix, in the z-plane onto two concentric circles with radii $R = \frac{x_1x_2 - 1 - \sqrt{(x_1^2-1)(x_2^2-1)}}{x_1 - x_2}$ and 1 respectively in the ζ-plane. The right inclusion S_1 is mapped onto a circular region $|\zeta| < R$; the matrix S_2 is mapped onto an annulus $R < |\zeta| < 1$, and the point at infinity $z = \infty$ is mapped to the point $\zeta = 1/a$; the left inclusion S_3 is mapped onto the region outside the unit circle, i.e., $|\zeta| > 1$.

The boundary conditions on the interface L_1 between the right circular inclusion and the matrix are given as follows:

$$\begin{aligned}
&\sigma_{rr}^{(1)} = \sigma_{rr}^{(2)} = \eta_1(\theta_1)(u_r^{(2)} - u_r^{(1)} - u_r^*),\\
&\sigma_{r\theta}^{(1)} = \sigma_{r\theta}^{(2)} = \eta_1(\theta_1)(u_\theta^{(2)} - u_\theta^{(1)} - u_\theta^*), \quad (|\zeta| = R).
\end{aligned} \tag{6}$$

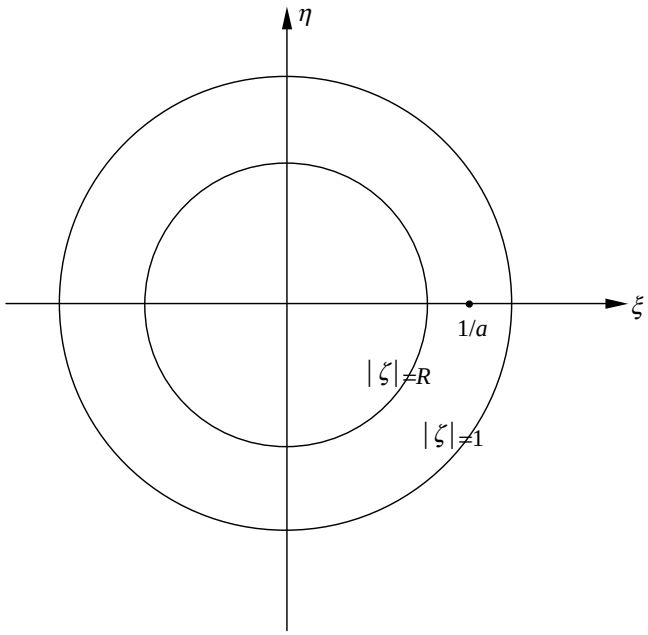

Fig. 2. Conformal mapping from the physical z-plane to the ζ-plane.

The boundary conditions on the interface L_2 between the left circular inclusion and the matrix are given as follows:

$$\begin{aligned}\sigma_{rr}^{(2)} &= \sigma_{rr}^{(3)} = -\eta_2(\theta_2)(u_r^{(2)} - u_r^{(3)} - u_r^{**}),\\ \sigma_{r\theta}^{(2)} &= \sigma_{r\theta}^{(3)} = -\eta_2(\theta_2)(u_\theta^{(2)} - u_\theta^{(3)} - u_\theta^{**}),\end{aligned} \quad (|\zeta| = 1), \tag{7}$$

where u^* is the displacement induced by the uniform eigenstrains $\{\varepsilon_x^*, \varepsilon_y^*, \varepsilon_{xy}^*\}$ prescribed within the right inclusion, while u^{**} is the displacement induced by the uniform eigenstrains $\{\varepsilon_x^{**}, \varepsilon_y^{**}, \varepsilon_{xy}^{**}\}$ prescribed within the left inclusion.$\eta_1(\theta_1)$ and $\eta_2(\theta_2)$ are two non-negative periodic functions of the angles θ_1 and θ_2, respectively.Physically, Eqs.(6) and (7) imply that the same degree of imperfection is realized in both the normal and tangential directions, and that the displacement jump across the interfaces L_1 and L_2 is in the same direction as the corresponding tractions.This kind of imperfect interface has also been adopted by Achenbach and Zhu (1990) and Sudak et al. (1999).Employing this type of imperfect interface, Sudak et al. (1999) showed that replacing the inhomogeneous interface by its homogeneous counterpart will lead to significant errors in even the calculation of the average stresses induced within the inclusion.The numerical results of Shen et al. (2001a,b) and Liu et al. (2001) also showed the importance of this kind of imperfect interface for application.Another reason for adopting this kind of imperfect interfaces is that since the stress field within an isolated circular inclusion with a homogeneous imperfect interface is still uniform (see Gao, 1995; Bigoni et al., 1998; Ru, 1998; Sudak et al., 1999), then the effects of circumferential inhomogeneity of the interface and perturbation caused by the neighboring inclusion can be easily noticed.L_1 (or L_2) is perfect when $\eta_1(\theta_1) = \infty$ (or $\eta_2(\theta_2) = \infty$); L_1 (or L_2) is completely debonded when setting $\eta_1(\theta_1) = 0$ (or$\eta_2(\theta_2) = 0$). Here, it shall be pointed out that the additional negative sign "−" appearing in Eq. (7) is due to the fact that the mapping function $m(\zeta)$ given by (4) maps the circular domain $|z| < 1$ in the z-plane onto the domain $|\zeta| > 1$ in the ζ-plane.

The unbounded matrix is subject to remote uniform loading $(\sigma_{xx}^\infty, \sigma_{xy}^\infty, \sigma_{yy}^\infty)$. Hence, the aim of this study is to determine three pairs of analytic functions $\phi_1(\zeta)$, $\psi_1(\zeta)$, $\phi_2(\zeta)$, $\psi_2(\zeta)$ and $\phi_3(\zeta)$, $\psi_3(\zeta)$ which satisfy the boundary conditions (6) and (7) on the two interfaces L_1, L_2 as well as the remote loading conditions.

To treat the boundary conditions on L_1, we introduce the following analytic continuation (England, 1971)

$$\begin{aligned}\phi_1(\zeta) &= -\frac{m(\zeta)}{\overline{m}'(R^2/\zeta)}\overline{\phi}_1'(R^2/\zeta) - \overline{\psi}_1(R^2/\zeta), \quad (|\zeta| > R),\\ \phi_2(\zeta) &= -\frac{m(\zeta)}{\overline{m}'(R^2/\zeta)}\overline{\phi}_2'(R^2/\zeta) - \overline{\psi}_2(R^2/\zeta), \quad (R^2 < |\zeta| < R).\end{aligned} \tag{8}$$

Similarly, we introduce the following analytic continuation to treat the boundary conditions on L_2

$$\begin{aligned}\phi_3(\zeta) &= -\frac{m(\zeta)}{\overline{m}'(1/\zeta)}\overline{\phi}_3'(1/\zeta) - \overline{\psi}_3(1/\zeta), \quad (|\zeta| < 1),\\ \phi_2(\zeta) &= -\frac{m(\zeta)}{\overline{m}'(1/\zeta)}\overline{\phi}_2'(1/\zeta) - \overline{\psi}_2(1/\zeta), \quad (1 < |\zeta| < 1/R).\end{aligned} \tag{9}$$

3. Satisfaction of boundary condition on L_1

In view of Eq. (8), the continuity condition of tractions across the interface $|t| = R$ can be expressed as

$$\phi_1^+(t) - \phi_1^-(t) = \phi_2^-(t) - \phi_2^+(t), \quad (|t| = R), \tag{10}$$

where the superscripts "+" and "−" denote the limit values from the inner and outer sides of the contour being considered.

A rearrangement of the above equation will yield

$$[\phi_1(t) + \phi_2(t)]^+ = [\phi_1(t) + \phi_2(t)]^-, \quad (|t| = R). \tag{11}$$

By the generalized Liouville's theorem, we obtain

$$\phi_1(\zeta) + \phi_2(\zeta) = \sum_{n=1}^{+\infty}(A_n\zeta^n + A_{-n}\zeta^{-n}) + \frac{D_1 + \Gamma_1}{\zeta - 1/a} + \frac{R^2\Gamma_2}{\zeta - aR^2}, \quad (R^2 < |\zeta| < 1), \tag{12}$$

where $A_{\pm n}$ $(n = 1, 2, 3, \ldots, +\infty)$ and D_1 are unknown coefficients, and

$$\Gamma_1 = (a^{-2} - 1)\frac{\sigma_{xx}^\infty + \sigma_{yy}^\infty}{4}, \quad \Gamma_2 = (1 - a^2)\frac{\sigma_{yy}^\infty - \sigma_{xx}^\infty - 2\mathrm{i}\sigma_{xy}^\infty}{2}, \tag{13}$$

$$D_1 = \frac{(a^2R^2 - 1)^2}{a^2}\overline{\phi_1'(aR^2)}. \tag{14}$$

The proportional relationship between tractions and displacement jumps on the interface $|t| = R$ can be expressed as

$$\begin{aligned}&\frac{(at - 1)(aR^2t^{-1} - 1)}{\eta_1(\theta_1)R(a^2 - 1)}t[\phi_1'^+(t) - \phi_1'^-(t)]\\ &\quad = \frac{\kappa_2}{2\mu_2}\phi_2^-(t) + \frac{1}{2\mu_2}\phi_2^+(t) - \frac{\kappa_1}{2\mu_1}\phi_1^+(t) - \frac{1}{2\mu_1}\phi_1^-(t) + \frac{\varepsilon_1^*}{t - 1/a} + \frac{R^2\varepsilon_2^*}{t - aR^2}, \quad (|t| = R),\end{aligned} \tag{15}$$

where

$$\varepsilon_1^* = \frac{1 - a^{-2}}{2}(\varepsilon_x^* + \varepsilon_y^*), \quad \varepsilon_2^* = \frac{1 - a^2}{2}(\varepsilon_x^* - \varepsilon_y^* + 2\mathrm{i}\varepsilon_{xy}^*). \tag{16}$$

Next, we employ the following approximate relationship for the inhomogeneously imperfect interface L_1 used in Wang and Shen (2002)

$$\frac{2\mu_1\mu_2}{\kappa_1\mu_2+\mu_1}\frac{1}{\eta_1(\theta_1)} \approx \lambda_1(1+a_1\cos\theta_1+b_1\sin\theta_1) = \lambda_1\frac{R(a^2-1)(p_0+p_1t+\overline{p}_1R^2t^{-1})}{(at-1)(aR^2t^{-1}-1)}, \quad (|t|=R), \tag{17}$$

where

$$\lambda_1>0, \quad a_1^2+b_1^2<1, \quad d=-\frac{1}{R}, \quad Y_1=\frac{a_1-ib_1}{2}, \tag{18}$$

$$p_0=\frac{1+a^2R^2+2aR^2d(Y_1+\overline{Y_1})}{R(a^2-1)}, \quad p_1=\frac{a+d(Y_1+a^2R^2\overline{Y_1})}{R(1-a^2)}. \tag{19}$$

Physically, Eq. (17) implies that we only retain the fundamental terms in the Fourier series expansion of $\frac{1}{\eta_1(\theta_1)}$, which is also a periodic function of θ_1, and ignore all the other higher order terms in its Fourier series expansion. Here it shall be pointed out that Sudak et al. (1999) also derived explicit results for this specific variation of the interface parameter. Inserting expression Eq. (12) into Eq. (15) and eliminating $\phi_2^+(t)$ and $\phi_2^-(t)$, we obtain

$$\begin{aligned}
&\phi_1^+(t)+\lambda_1(p_0+p_1t+\overline{p}_1R^2t^{-1})t\phi_1'^+(t)-\beta_1\sum_{n=1}^{+\infty}A_nt^n-\frac{\beta_1\Pi_1+(\beta_1-\delta_1)D_1}{t-1/a}+\frac{D_1\lambda_1t(p_0+p_1t+\overline{p}_1R^2t^{-1})}{(t-1/a)^2}\\
&\quad=-\delta_1\phi_1^-(t)+\lambda_1(p_0+p_1t+\overline{p}_1R^2t^{-1})t\phi_1'^-(t)+\beta_1\sum_{n=1}^{+\infty}A_{-n}t^{-n}\\
&\qquad+\frac{\beta_1R^2\Pi_2}{t-aR^2}+\frac{\delta_1D_1}{t-1/a}+\frac{D_1\lambda_1t(p_0+p_1t+\overline{p}_1R^2t^{-1})}{(t-1/a)^2}, \quad (|t|=R),
\end{aligned} \tag{20}$$

where

$$\delta_1=\frac{\kappa_2\mu_1+\mu_2}{\kappa_1\mu_2+\mu_1}, \quad \beta_1=\frac{\kappa_2\mu_1+\mu_1}{\kappa_1\mu_2+\mu_1}, \quad \Pi_1=\Gamma_1+\frac{2\mu_2}{\kappa_2+1}\varepsilon_1^*, \quad \Pi_2=\Gamma_2+\frac{2\mu_2}{\kappa_2+1}\varepsilon_2^*. \tag{21}$$

It can be observed that the left-hand side of Eq. (20) is analytic and single-valued within the circle $|t|=R$; while the right-hand side of Eq. (21) is analytic and single-valued outside the circle $|t|=R$ including the point at infinity. By the Liouville's theorem, we can arrive at the following two first-order differential equations with variable coefficients for $\phi_1(\zeta)$

$$\begin{aligned}
&\phi_1(\zeta)+\lambda_1(p_0+p_1\zeta+\overline{p}_1R^2\zeta^{-1})\zeta\phi_1'(\zeta)\\
&\quad=\beta_1\sum_{n=1}^{+\infty}A_n\zeta^n+\frac{\beta_1\Pi_1+(\beta_1-\delta_1)D_1}{\zeta-1/a}-\frac{D_1\lambda_1\zeta(p_0+p_1\zeta+\overline{p}_1R^2\zeta^{-1})}{(\zeta-1/a)^2}, \quad (|\zeta|<R),\\
&\delta_1\phi_1(\zeta)-\lambda_1(p_0+p_1\zeta+\overline{p}_1R^2\zeta^{-1})\zeta\phi_1'(\zeta)\\
&\quad=\beta_1\sum_{n=1}^{+\infty}A_{-n}\zeta^{-n}+\frac{\beta_1R^2\Pi_2}{\zeta-aR^2}+\frac{\delta_1D_1}{\zeta-1/a}+\frac{D_1\lambda_1\zeta(p_0+p_1\zeta+\overline{p}_1R^2\zeta^{-1})}{(\zeta-1/a)^2}, \quad (|\zeta|>R).
\end{aligned} \tag{22}$$

Next let $\phi_1(\zeta)$ be expanded into the following power series forms

$$\begin{aligned}
&\phi_1(\zeta)=\sum_{n=1}^{+\infty}B_n\zeta^n, \quad (|\zeta|<R),\\
&\phi_1(\zeta)=\frac{D_1}{\zeta-1/a}+\sum_{n=1}^{+\infty}B_{-n}\zeta^{-n}, \quad (|\zeta|>R).
\end{aligned} \tag{23}$$

Here it shall be noted that $\phi_1(\zeta)$ ($|\zeta| > R$) has a first-order pole at $\zeta = 1/a$. The first order pole is due to the analytic continuation defined by Eq. (8). The consistency condition Eq. (14) for $\phi_1(\zeta)$ ($|\zeta| < R$) at the point $\zeta = aR^2$ will result in the following equation

$$\sum_{n=1}^{+\infty} n(aR^2)^{n-1}B_n - \frac{a^2}{(a^2R^2-1)^2}\overline{D_1} = 0. \tag{24}$$

Substituting Eq. (23) into Eq. (22) and equating the coefficients of the same power of ζ, we obtain the following set of algebraic equations

$$\begin{aligned}
&\lambda_1 p_1 a^{-(n+1)}(n-1)B_{n-1} + a^{-(n+1)}(1+\lambda_1 p_0 n)B_n + \lambda_1\overline{p}_1 R^2 a^{-(n+1)}(n+1)B_{n+1} - \beta_1 a^{-(n+1)}A_n \\
&\quad + [(\beta_1-\delta_1) + \lambda_1 p_1 a^{-1}(n-1) + \lambda_1 p_0 n + \lambda_1\overline{p}_1 aR^2(n+1)]D_1 = -\beta_1\Pi_1, \\
&\lambda_1\overline{p}_1 R^2(n-1)B_{-(n-1)} + (\delta_1 + \lambda_1 p_0 n)B_{-n} + \lambda_1 p_1(n+1)B_{-(n+1)} \\
&\quad - \beta_1 A_{-n} = a^{n-1}R^{2n}\beta_1\Pi_2, \quad (n = 1,2,3,\ldots,+\infty).
\end{aligned} \tag{25}$$

Substituting Eq. (23) into Eq. (12), we obtain the following expressions for $\phi_2(\zeta)$

$$\begin{aligned}
\phi_2(\zeta) &= \sum_{n=1}^{+\infty}[(A_n - B_n)\zeta^n + A_{-n}\zeta^{-n}] + \frac{D_1+\Gamma_1}{\zeta - 1/a} + \frac{R^2\Gamma_2}{\zeta - aR^2}, \quad (R^2 < |\zeta| < R), \\
\phi_2(\zeta) &= \sum_{n=1}^{+\infty}[A_n\zeta^n + (A_{-n} - B_{-n})\zeta^{-n}] + \frac{\Gamma_1}{\zeta - 1/a} + \frac{R^2\Gamma_2}{\zeta - aR^2}, \quad (R < |\zeta| < 1).
\end{aligned} \tag{26}$$

The complex potentials $\phi_1(\zeta)$ and $\phi_2(\zeta)$ derived in this section have exactly satisfied the boundary conditions Eq. (6) on the interface L_1 as well as the remote loading conditions.

4. Satisfaction of boundary condition on L_2

In view of Eq. (9), the continuity condition of tractions across the interface $|\tau| = 1$ can be expressed as

$$\phi_2^+(\tau) - \phi_2^-(\tau) = \phi_3^-(\tau) - \phi_3^+(\tau), \quad (|\tau| = 1). \tag{27}$$

A rearrangement of the above equation will yield

$$[\phi_2(\tau) + \phi_3(\tau)]^+ = [\phi_2(\tau) + \phi_3(\tau)]^-, \quad (|\tau| = 1). \tag{28}$$

By the generalized Liouville's theorem, we obtain

$$\phi_2(\zeta) + \phi_3(\zeta) = \sum_{n=1}^{+\infty}(E_n\zeta^n + E_{-n}\zeta^{-n}) + \frac{D_2+\Gamma_1}{\zeta - 1/a} + \frac{\Gamma_2}{\zeta - a}, \quad \left(R < |\zeta| < \frac{1}{R}\right), \tag{29}$$

where $E_{\pm n}$ ($n = 1,2,3,\ldots,+\infty$) and D_2 are unknown coefficients, and

$$D_2 = \frac{(a^2-1)^2}{a^2}\overline{\phi_3'(a)}. \tag{30}$$

The proportional relationship between tractions and displacement jumps on the interface $|\tau| = 1$ can be expressed as

$$\begin{aligned}
&-\frac{(a\tau-1)(a\tau^{-1}-1)}{\eta_2(\theta_2)(a^2-1)}\tau[\phi_3'^-(\tau) - \phi_3'^+(\tau)] \\
&\quad = \frac{\kappa_2}{2\mu_2}\phi_2^+(\tau) + \frac{1}{2\mu_2}\phi_2^-(\tau) - \frac{\kappa_3}{2\mu_3}\phi_3^-(\tau) - \frac{1}{2\mu_3}\phi_3^+(\tau) + \frac{\varepsilon_1^{**}}{\tau - 1/a} + \frac{\varepsilon_2^{**}}{\tau - a}, \quad (|\tau| = 1),
\end{aligned} \tag{31}$$

where

$$\varepsilon_1^{**} = \frac{1-a^{-2}}{2}(\varepsilon_x^{**} + \varepsilon_y^{**}), \quad \varepsilon_2^{**} = \frac{1-a^2}{2}(\varepsilon_x^{**} - \varepsilon_y^{**} + 2\mathrm{i}\varepsilon_{xy}^{**}). \tag{32}$$

Next, we also employ the following approximate relationship for the inhomogeneously imperfect interface L_2 used in Wang and Shen (2002)

$$\frac{2\mu_2\mu_3}{\kappa_3\mu_2+\mu_3}\frac{1}{\eta_2(\theta_2)} \approx \lambda_2(1 + a_2\cos\theta_2 + b_2\sin\theta_2) = \lambda_2\frac{(a^2-1)(q_0+q_1\tau+\overline{q}_1\tau^{-1})}{(a\tau-1)(a\tau^{-1}-1)}, \quad (|\tau|=1), \tag{33}$$

where

$$\lambda_2 > 0, \quad a_2^2 + b_2^2 < 1, \quad Y_2 = \frac{a_2 - \mathrm{i}b_2}{2}, \tag{34}$$

$$q_0 = \frac{1 + a^2 + 2a(Y_2 + \overline{Y_2})}{a^2-1}, \quad q_1 = \frac{a + Y_2 + a^2\overline{Y_2}}{1-a^2}. \tag{35}$$

Physically, Eq. (33) implies that we only retain the fundamental terms in the Fourier series expansion of $\frac{1}{\eta_2(\theta_2)}$, which is also a periodic function of θ_2, and ignore all the other higher order terms in its Fourier series expansion. Inserting expression Eq. (29) into Eq. (31) and eliminating $\phi_2^+(\tau)$ and $\phi_2^-(\tau)$, we obtain

$$\begin{aligned}
&\phi_3^-(\tau) - \lambda_2(q_0 + q_1\tau + \overline{q}_1\tau^{-1})\tau\phi_3'^-(\tau) - \beta_2\sum_{n=1}^{+\infty}E_{-n}\tau^{-n} - \frac{\beta_2\Lambda_1 + (\beta_2-\delta_2)D_2}{\tau - 1/a} - \frac{D_2\lambda_2\tau(q_0+q_1\tau+\overline{q}_1\tau^{-1})}{(\tau-1/a)^2} \\
&= -\delta_2\phi_3^+(\tau) - \lambda_2(q_0 + q_1\tau + \overline{q}_1\tau^{-1})\tau\phi_3'^+(\tau) + \beta_2\sum_{n=1}^{+\infty}E_n\tau^n + \frac{\beta_2\Lambda_2}{\tau-a} + \frac{\delta_2 D_2}{\tau-1/a} \\
&\quad - \frac{D_2\lambda_2\tau(q_0+q_1\tau+\overline{q}_1\tau^{-1})}{(\tau-1/a)^2}, \quad (|\tau|=1),
\end{aligned} \tag{36}$$

where

$$\delta_2 = \frac{\kappa_2\mu_3+\mu_2}{\kappa_3\mu_2+\mu_3}, \quad \beta_2 = \frac{\kappa_2\mu_3+\mu_3}{\kappa_3\mu_2+\mu_3}, \quad \Lambda_1 = \Gamma_1 + \frac{2\mu_2}{\kappa_2+1}\varepsilon_1^{**}, \quad \Lambda_2 = \Gamma_2 + \frac{2\mu_2}{\kappa_2+1}\varepsilon_2^{**}. \tag{37}$$

It can be observed that the right-hand side of Eq. (36) is analytic and single-valued within the unit circle $|\tau| = 1$; while the left-hand side of Eq. (36) is analytic and single-valued outside the unit circle $|\tau| = 1$ including the point at infinity. By the Liouville's theorem, we can arrive at the following two first-order differential equations with variable coefficients for $\phi_3(\zeta)$

$$\begin{aligned}
&\phi_3(\zeta) - \lambda_2(q_0 + q_1\zeta + \overline{q}_1\zeta^{-1})\zeta\phi_3'(\zeta) \\
&\quad = \beta_2\sum_{n=1}^{+\infty}E_{-n}\zeta^{-n} + \frac{\beta_2\Lambda_1 + (\beta_2-\delta_2)D_2}{\zeta-1/a} + \frac{D_2\lambda_2\zeta(q_0+q_1\zeta+\overline{q}_1\zeta^{-1})}{(\zeta-1/a)^2}, \quad (|\zeta|>1), \\
&\delta_2\phi_3(\zeta) + \lambda_2(q_0 + q_1\zeta + \overline{q}_1\zeta^{-1})\zeta\phi_3'(\zeta) \\
&\quad = \beta_2\sum_{n=1}^{+\infty}E_n\zeta^n + \frac{\beta_2\Lambda_2}{\zeta-a} + \frac{\delta_2 D_2}{\zeta-1/a} - \frac{D_2\lambda_2\zeta(q_0+q_1\zeta+\overline{q}_1\zeta^{-1})}{(\zeta-1/a)^2}, \quad (|\zeta|<1).
\end{aligned} \tag{38}$$

Let $\phi_3(\zeta)$ be expanded into the following power series form

$$\begin{aligned}
&\phi_3(\zeta) = \sum_{n=1}^{+\infty}F_{-n}\zeta^{-n}, \qquad (|\zeta|>1), \\
&\phi_3(\zeta) = \tfrac{D_2}{\zeta-1/a} + \sum_{n=1}^{+\infty}F_n\zeta^n, \quad (|\zeta|<1).
\end{aligned} \tag{39}$$

Here it shall be noted that $\phi_3(\zeta)$ ($|\zeta| < 1$) has a first-order pole at $\zeta = 1/a$. The first-order pole is due to the analytic continuation defined by Eq. (9). The consistency condition Eq. (30) for $\phi_3(\zeta)$ ($|\zeta| > 1$) at the point $\zeta = a$ will result in the following equation

$$\sum_{n=1}^{+\infty} n a^{-n-1} F_{-n} + \frac{a^2}{(a^2-1)^2}\overline{D_2} = 0. \tag{40}$$

Substituting Eq. (39) into Eq. (38) and equating the coefficients of the same power of ζ, we obtain the following set of algebraic equations

$$\begin{aligned}
&\lambda_2\overline{q}_1(n-1)F_{-(n-1)} + (1+\lambda_2 q_0 n)F_{-n} + \lambda_2 q_1(n+1)F_{-(n+1)} - \beta_2 E_{-n} - a^{-n}[a(\beta_2-\delta_2) + \lambda_2\overline{q}_1(n-1)a^2 \\
&\quad + \lambda_2 q_0 n a + \lambda_2 q_1(n+1)]D_2 = a^{-(n-1)}\beta_2\Lambda_1, \\
&\lambda_2 q_1(n-1)F_{n-1} + (\delta_2 + \lambda_2 q_0 n)F_n + \lambda_2\overline{q}_1(n+1)F_{n+1} - \beta_2 E_n = -a^{-(n+1)}\beta_2\Lambda_2, \\
&\quad (n = 1, 2, 3, \ldots, +\infty).
\end{aligned} \tag{41}$$

Substituting Eq. (39) into Eq. (29), we obtain the following expressions for $\phi_2(\zeta)$

$$\begin{aligned}
\phi_2(\zeta) &= \sum_{n=1}^{+\infty}[E_n\zeta^n + (E_{-n} - F_{-n})\zeta^{-n}] + \tfrac{D_2+\Gamma_1}{\zeta-1/a} + \tfrac{\Gamma_2}{\zeta-a}, \quad (1 < |\zeta| < \tfrac{1}{R}), \\
\phi_2(\zeta) &= \sum_{n=1}^{+\infty}[(E_n - F_n)\zeta^n + E_{-n}\zeta^{-n}] + \tfrac{\Gamma_1}{\zeta-1/a} + \tfrac{\Gamma_2}{\zeta-a}, \qquad (R < |\zeta| < 1).
\end{aligned} \tag{42}$$

The complex potentials $\phi_2(\zeta)$ and $\phi_3(\zeta)$ derived above have exactly satisfied the boundary conditions Eq. (7) on the interface L_2 as well as the remote loading conditions.

5. Compatibility condition for $\phi_2(\zeta)$ and $\psi_2(\zeta)$

In order to simultaneously satisfy the boundary conditions on the interfaces L_1 and L_2, the compatibility condition for ϕ_2 (ζ) and $\psi_2(\zeta)$ ($R < |\zeta| < 1$) shall be satisfied. The compatibility condition for $\phi_2(\zeta)$ ($R < |\zeta| < 1$) will result into the following two identities

$$\begin{aligned}
&\sum_{n=1}^{+\infty}(A_n - E_n + F_n)\zeta^n = \frac{\Gamma_2}{\zeta - a}, \\
&\sum_{n=1}^{+\infty}(-A_{-n} + B_{-n} + E_{-n})\zeta^{-n} = \frac{R^2\Gamma_2}{\zeta - aR^2}, \qquad (R < |\zeta| < 1).
\end{aligned} \tag{43}$$

Expanding the two first-order poles $\zeta = a$ and $\zeta = aR^2$ in Eq. (43), both of which are located outside the annulus $R < |\zeta| < 1$, and equating the coefficients for the same power of ζ, we can obtain the following set of algebraic equations

$$\begin{aligned}
&A_n - E_n + F_n = -a^{-(n+1)}\Gamma_2, \\
&A_{-n} - B_{-n} - E_{-n} = -a^{n-1}R^{2n}\Gamma_2, \quad (n = 1, 2, 3, \ldots, +\infty).
\end{aligned} \tag{44}$$

The compatibility condition for $\psi_2(\zeta)$ ($R < |\zeta| < 1$) will result in the following identity

$$\overline{\phi}_2(1/\zeta) - \overline{\phi}_2(R^2/\zeta) + \frac{(1-R^2)(a\zeta-1)^2}{(\zeta-a)(\zeta-aR^2)}\zeta\phi_2'(\zeta) + \overline{K} = 0, \quad (R < |\zeta| < 1), \tag{45}$$

where the unknown constant K, which represents the rigid body displacement, must be included in the compatibility condition for $\psi_2(\zeta)$.

The above expression Eq. (45) can be written equivalently as

$$[\zeta^2 - a(1+R^2)\zeta + (aR)^2][\overline{K} + \overline{\phi}_2(1/\zeta) - \overline{\phi}_2(R^2/\zeta)] + (1-R^2)(a^2\zeta^2 - 2a\zeta + 1)\zeta\phi_2'(\zeta) = 0 \quad (R < |\zeta| < 1). \tag{46}$$

Substituting Eqs. (26) and (42) into Eq. (46), and making use of Eq. $(44)_1$, we can finally obtain

$$\begin{aligned}&[\zeta^2 - a(1+R^2)\zeta + (aR)^2]\sum_{n=1}^{+\infty}\left\{(-\overline{A_{-n}}R^{-2n} + \overline{E_{-n}} - \overline{F_{-n}})\zeta^n + [(-\overline{A_n} + \overline{B_n})R^{2n} + \overline{E_n}]\zeta^{-n}\right\}\\ &+ (1-R^2)(a^2\zeta^2 - 2a\zeta + 1)\sum_{n=1}^{+\infty} n[A_n\zeta^n - E_{-n}\zeta^{-n}] + \overline{K}\zeta^2 + [a^2R^2\overline{D_1} - a^2\overline{D_2} - 2a^2(1-R^2)\Gamma_1\\ &- a(1+R^2)\overline{K}]\zeta + a^3R^2(\overline{D_2} - \overline{D_1}) + (aR)^2\overline{K} = 0 \quad (R < |\zeta| < 1).\end{aligned} \tag{47}$$

Equating the coefficients for the same power of ζ in Eq. (47), we can obtain the following set of algebraic equations

$$\begin{aligned}&aR^2(1+R^2)A_1 - R^4A_2 - aR^2(1+R^2)B_1 + R^4B_2 - a(1+R^2)E_1 + E_2 + 2a(1-R^2)\overline{E_{-1}} - 2a^2(1-R^2)\overline{E_{-2}}\\ &- a^3R^2D_1 + a^3R^2D_2 + (aR)^2K = 0,\end{aligned} \tag{48}$$

$$\begin{aligned}&-a^2A_{-1} + (aR)^2E_{-1} - (aR)^2F_{-1} - R^2A_1 + R^2B_1 + E_1 + (1-R^2)\overline{A_1} - a^2(1-R^2)\overline{E_{-1}} + a^2R^2D_1\\ &- a^2D_2 - a(1+R^2)K = 2a^2(1-R^2)\Gamma_1,\end{aligned} \tag{49}$$

$$\begin{aligned}&a(1+R^{-2})A_{-1} - a^2R^{-2}A_{-2} - a(1+R^2)E_{-1} + (aR)^2E_{-2} + a(1+R^2)F_{-1} - (aR)^2F_{-2} - 2a(1-R^2)\overline{A_1}\\ &+ 2(1-R^2)\overline{A_2} + K = 0,\end{aligned} \tag{50}$$

$$\begin{aligned}&-A_{-n} + a(1+R^{-2})A_{-(n+1)} - a^2R^{-2}A_{-(n+2)} + R^{2n}E_{-n} - a(1+R^2)R^{2n}E_{-(n+1)} + a^2R^{2(n+1)}E_{-(n+2)}\\ &- R^{2n}F_{-n} + a(1+R^2)R^{2n}F_{-(n+1)} - a^2R^{2(n+1)}F_{-(n+2)} + (1-R^2)R^{2n}[a^2n\overline{A_n} - 2a(n+1)\overline{A_{n+1}}\\ &+ (n+2)\overline{A_{n+2}}] = 0, \quad (n = 1,2,3,\ldots,+\infty),\end{aligned} \tag{51}$$

$$\begin{aligned}&-a^2R^{2(n+1)}A_n + aR^{2(n+1)}(1+R^2)A_{n+1} - R^{2(n+2)}A_{(n+2)} + a^2R^{2(n+1)}B_n - aR^{2(n+1)}(1+R^2)B_{n+1}\\ &+ R^{2(n+2)}B_{(n+2)} + (aR)^2E_n - a(1+R^2)E_{n+1} + E_{n+2} - (1-R^2)[n\overline{E_{-n}} - 2a(n+1)\overline{E_{-(n+1)}}\\ &+ a^2(n+2)\overline{E_{-(n+2)}}] = 0, \quad (n = 1,2,3,\ldots,+\infty).\end{aligned} \tag{52}$$

6. Explicit expressions for complex potentials

Associating Eq. (24), (25), (40), (41), (44), (48)–(52) and truncating the infinite system of algebraic equations at a sufficiently large integer, we can get $2\times(8N+3)$ independent linear equations for the $8N+3$ unknowns $A_{\pm n}, B_{\pm n}, E_{\pm n}, F_{\pm n}, D_1, D_2, K$ $(n = 1,2,3,\ldots,N)$ and their conjugates. These unknown coefficients can then be uniquely determined. Now the explicit expressions for the three pairs of complex potentials $\phi_1(\zeta), \psi_1(\zeta), \phi_2(\zeta), \psi_2(\zeta)$ and $\phi_3(\zeta), \psi_3(\zeta)$ are given by

$$\begin{aligned}
\phi_1(\zeta) &= \sum_{n=1}^{+\infty} B_n \zeta^n, \\
\psi_1(\zeta) &= -\sum_{n=1}^{+\infty} R^{-2n}\overline{B_{-n}}\zeta^n - \frac{(a\zeta - R^2)(a\zeta - 1)^2 \sum_{n=1}^{+\infty} nB_n\zeta^{n-1}}{(a^2-1)(\zeta - aR^2)} + \frac{a^2R^2\overline{D_1}}{\zeta - aR^2},
\end{aligned} \qquad (|\zeta| < R), \tag{53}$$

$$\begin{aligned}
\phi_2(\zeta) &= \sum_{n=1}^{+\infty}[(E_n - F_n)\zeta^n + E_{-n}\zeta^{-n}] + \tfrac{\Gamma_2}{\zeta - a} + \tfrac{\Gamma_1}{\zeta - 1/a}, \\
\psi_2(\zeta) &= -\sum_{n=1}^{+\infty}[\overline{E_n}\zeta^{-n} + (\overline{E_{-n}} - \overline{F_{-n}})\zeta^n] \\
&\quad - \frac{(a\zeta - 1)^3 \sum_{n=1}^{+\infty} n[(E_n - F_n)\zeta^n - E_{-n}\zeta^{-n}]}{(a^2-1)\zeta(\zeta - a)} \\
&\quad + \frac{a^2(\overline{D_2} + 2\Gamma_1)}{\zeta - a} + \frac{(a\zeta - 1)^3\Gamma_2}{(a^2-1)(\zeta - a)^3} + \frac{\overline{\Gamma_2}}{a(a\zeta - 1)},
\end{aligned} \qquad (R < |\zeta| < 1), \tag{54}$$

$$\begin{aligned}
\phi_3(\zeta) &= \sum_{n=1}^{+\infty} F_{-n}\zeta^{-n}, \\
\psi_3(\zeta) &= -\sum_{n=1}^{+\infty} \overline{F_n}\zeta^{-n} + \frac{(a\zeta - 1)^3 \sum_{n=1}^{+\infty} nF_{-n}\zeta^{-n-1}}{(a^2-1)(\zeta - a)} + \frac{a^2\overline{D_2}}{\zeta - a},
\end{aligned} \qquad (|\zeta| > 1). \tag{55}$$

As a check, we consider the special case in which the right inclusion possesses the same elastic properties as those of the matrix, and the interface L_1 is a perfect interface, i.e., $\eta_1(\theta_1) \to +\infty$. In addition, the imperfect interface L_2 is assumed to be homogeneous, i.e., $a_2 = b_2 = 0$. For this case, it can be deduced that $E_{\pm n} = 0$ $(n = 1, 2, \ldots, +\infty)$. Consequently, we will have

$$\begin{aligned}
\phi_3(\zeta) &= \frac{\beta_2\Lambda_1}{\beta_2 - \delta_2 + 2\lambda_2 + 1}\frac{1}{\zeta - 1/a}, \\
\psi_3(\zeta) &= \frac{\beta_2\overline{\Lambda}_2}{a^2(\delta_2 + \lambda_2)}\frac{1}{\zeta - 1/a},
\end{aligned} \qquad |\zeta| > 1, \tag{56}$$

which implies that the stress field within the left circular inclusion is uniform. More precisely, the uniform stress field is given by

$$\begin{aligned}
\sigma_{xx} + \sigma_{yy} &= \frac{\beta_2}{\beta_2 - \delta_2 + 2\lambda_2 + 1}\left[\sigma^\infty_{xx} + \sigma^\infty_{yy} - \frac{4\mu_2}{\kappa_2 + 1}(\varepsilon^{**}_x + \varepsilon^{**}_y)\right], \\
\sigma_{yy} - \sigma_{xx} + 2\mathrm{i}\sigma_{xy} &= \frac{\beta_2}{\delta_2 + \lambda_2}\left[\sigma^\infty_{yy} - \sigma^\infty_{xx} + 2\mathrm{i}\sigma^\infty_{xy} + \frac{2\mu_2}{\kappa_2 + 1}(\varepsilon^{**}_x - \varepsilon^{**}_y - 2\mathrm{i}\varepsilon^{**}_{xy})\right].
\end{aligned} \tag{57}$$

The above results are in agreement with those given by Gao (1995), Bigoni et al. (1998), Ru (1998) and Sudak et al. (1999).

It can also be observed from the above analysis that the non-uniform stresses within each circular inclusion are caused by two factors. One factor is the inhomogeneity of the imperfect interfaces, another one comes from the perturbation caused by the neighboring circular inclusion.

7. Stress field

The stress field in the two inclusions and the matrix can be expressed in terms of the obtained complex potentials $\phi_k(\zeta), \psi_k(\zeta)$ $(k = 1, 2, 3)$ as follows:

$$\begin{aligned}
\sigma_{xx}^{(k)} &= \mathrm{Re}\left\{2\frac{\phi_k'(\zeta)}{m'(\zeta)} - \overline{m(\zeta)}\left\{\frac{\phi_k'(\zeta)}{m'(\zeta)}\right\}' - \frac{\psi_k'(\zeta)}{m'(\zeta)}\right\},\\
\sigma_{yy}^{(k)} &= \mathrm{Re}\left\{2\frac{\phi_k'(\zeta)}{m'(\zeta)} + \overline{m(\zeta)}\left\{\frac{\phi_k'(\zeta)}{m'(\zeta)}\right\}' + \frac{\psi_k'(\zeta)}{m'(\zeta)}\right\}, \quad \text{with } k = 1, 2, 3.\\
\sigma_{xy}^{(k)} &= \mathrm{Im}\left\{\overline{m(\zeta)}\left\{\frac{\phi_k'(\zeta)}{m'(\zeta)}\right\}' + \frac{\psi_k'(\zeta)}{m'(\zeta)}\right\}.
\end{aligned} \tag{58}$$

The tractions along the two interfaces L_1 and L_2 are given by

$$\sigma_{rr} + \mathrm{i}\sigma_{r\theta} = \frac{(a\zeta - 1)^2}{a^2 - 1}\sum_{n=1}^{+\infty} n(B_n\zeta^{n-1} + B_{-n}\zeta^{-n-1}) + \frac{a^2 D_1}{a^2 - 1}, \quad (\zeta \in L_1), \tag{59}$$

$$\sigma_{rr} + \mathrm{i}\sigma_{r\theta} = \frac{(a\zeta - 1)^2}{1 - a^2}\sum_{n=1}^{+\infty} n(F_n\zeta^{n-1} + F_{-n}\zeta^{-n-1}) + \frac{a^2 D_2}{a^2 - 1}, \quad (\zeta \in L_2). \tag{60}$$

The mean stresses on the inclusion side of the two interfaces are

$$\sigma_{rr}^{(1)} + \sigma_{\theta\theta}^{(1)} = \frac{2}{a^2 - 1}\mathrm{Re}\left\{\sum_{n=1}^{+\infty} n(a\zeta - 1)^2 B_n\zeta^{n-1}\right\}, \quad (\zeta \in L_1), \tag{61}$$

$$\sigma_{rr}^{(3)} + \sigma_{\theta\theta}^{(3)} = \frac{2}{1 - a^2}\mathrm{Re}\left\{\sum_{n=1}^{+\infty} n(a\zeta - 1)^2 F_{-n}\zeta^{-n-1}\right\}, \quad (\zeta \in L_2). \tag{62}$$

The resultant traction $\sigma_{\text{resultant}}$ on the two interfaces L_1 and L_2, which is important in understanding the relationship between the imperfect interface parameters $\eta_1(\theta_1)$, $\eta_2(\theta_2)$ and the failure of the interface (Shen et al., 2001a,b), is defined by

$$\sigma_{\text{resultant}} = \sqrt{\sigma_{rr}^2 + \sigma_{r\theta}^2} = |\sigma_{rr} + \mathrm{i}\sigma_{r\theta}|, \quad (\zeta \in L_1 \cup L_2). \tag{63}$$

The average stresses inside each inclusion also give important information regarding the overall understanding and behavior of the composite material. For example, the average stresses within the left circular inclusion are calculated to be

$$\begin{aligned}
&\overline{\sigma_{xx}} + \overline{\sigma_{yy}} = \frac{2a^2}{a^2 - 1}(D_2 + \overline{D_2}),\\
&\overline{\sigma_{yy}} - \overline{\sigma_{xx}} + 2\mathrm{i}\overline{\sigma_{xy}}\\
&\quad = -\frac{2a^4}{a^2 - 1}\overline{D_2} + 2(a^2 - 1)\sum_{n=1}^{+\infty} a^{-n-1} n\overline{F_n} - \frac{1}{3}(a^2 - 1)^2\sum_{n=1}^{+\infty} a^{-n-3} n(n+1)[(4-n)a^2 + n + 2]F_{-n},
\end{aligned} \tag{64}$$

where the over bar "– " on the left hand denotes the average value. We can observe that the two coefficients D_1 and D_2 are closely associated with the average mean stresses within the two inclusions.

8. Example

Before calculations and discussions, we should check the correctness of our results. Here we would like to point out that it is not feasible for us to make a direct comparison with the results of Mogilevskaya and Crouch (2002) since the fact that they only presented the results for a finite rectangular array of inclusions. There are two ways to check our result. First, we let the two inclusions of equal size with homogeneously imperfect interfaces be far away from each other so that the interaction between the two inclusions is minimal, the calculations demonstrate that uniform stress field within each inclusion is the same as that given by Eq. (57). Second, we let the two inclusions possess the same elastic properties and be of equal size. In

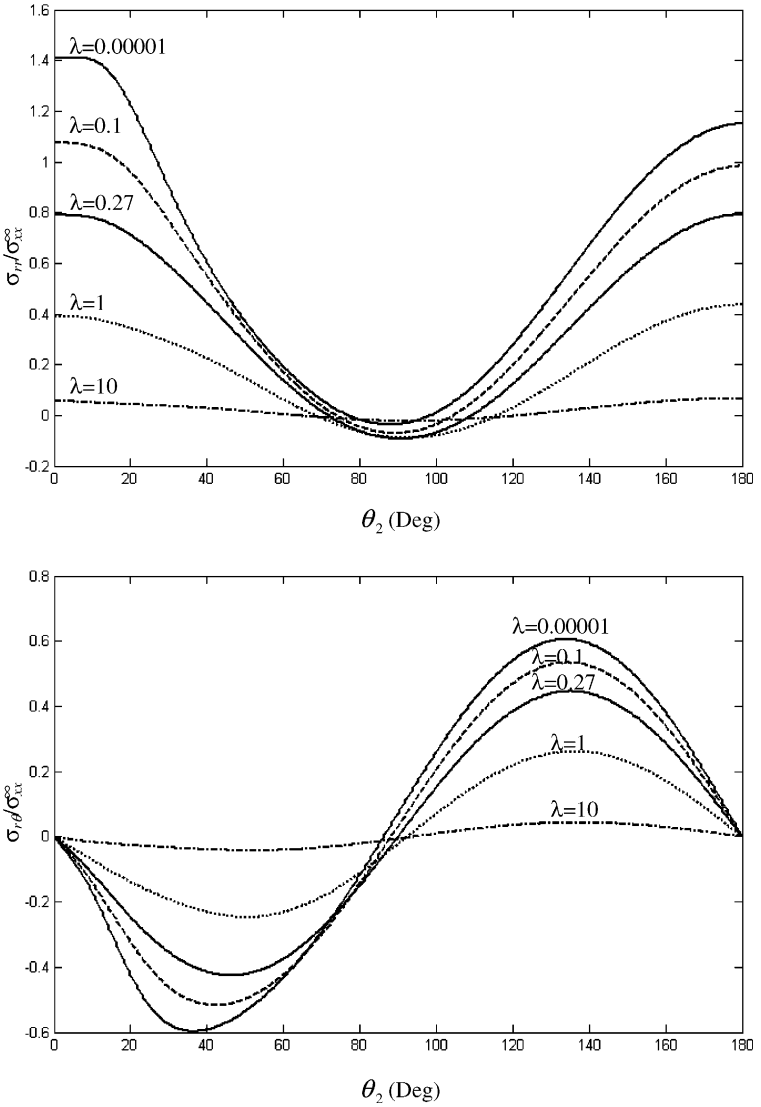

Fig. 3. Normal and tangential stresses along the left interface L_2 for different values of imperfect parameter λ when the remote stress is σ_{xx}^{∞}.

addition, the interface parameters are chosen to be $\lambda_1 = \lambda_2$ and $a_1 = -a_2$, $b_1 = b_2$. The numerical results show that the tractions on the two interfaces L_1 and L_2 are really symmetric with respect to the y_1-axis, which is parallel to the y-axis and passes through the point $((1 + x_2)/2, 0)$. In the following, remote uniform loadings and uniform eigenstrains imposed on the inclusions will be discussed separately.

8.1. Remote uniform loading

Let us consider the case of an aluminum matrix surrounding the left S-glass inclusion and the right silicon inclusion. This kind of composite materials is the so called three phase hybrid composite (Kanaun and Jeulin, 2001). The material properties of the matrix and the inclusions are described by (Shen et al., 2001a,b; Dvorak and Zhang, 2001)

$$\nu_2 = 0.33, \quad \mu_2 = 23.31 \text{ Gpa},$$
$$\nu_1 = 0.28, \quad \mu_1 = 74.22 \text{ Gpa},$$
$$\nu_3 = 0.24, \quad \mu_3 = 34.9 \text{ Gpa}.$$

Furthermore, we assume that $x_2 = 1.01$, $x_1 = 3.01$. In this case, the two inclusions are of equal size and closely spaced. In this calculation, the matrix is subject to uniaxial horizontal tension σ_{xx}^{∞}. In the following, we will probe the effects of interface imperfection characterized by λ_1,λ_2 and interface inhomogeneity characterized by a_1, a_2, b_1, b_2 on the interfacial stresses and average stresses within the inclusions.

First, we will consider homogeneous interfaces. In Fig. 3, the stress distribution along the left interface L_2 (normal and tangential directions) is plotted for different λ ($\lambda = \lambda_1 = \lambda_2$). It is observed from Fig. 3 that the stresses are not symmetric or anti-symmetric with respect to $\theta_2 = 90°$ due to the perturbation caused by the right inclusion. It is deduced from Fig. 3 that a negative normal displacement jump across L_2 may occur when $\theta_2 \approx 90°$. The physical ground for this seemingly unacceptable overlapping phenomenon has been explained by Shen et al. (2001a). One possible way to eliminate or alleviate the overlapping phenomenon may be the introduction of the interphase layer model (Mogilevskaya and Crouch, 2004). It is found that when $\lambda < 0.27$ (the interface is relatively perfect), the peak traction (the peak traction is found by calculating the maximum value of the resultant traction $\sigma_{\text{resultant}} = |\sigma_{rr} + \mathrm{i}\sigma_{r\theta}|$ along the interface) occurs at $\theta_2 = 0^0$; when

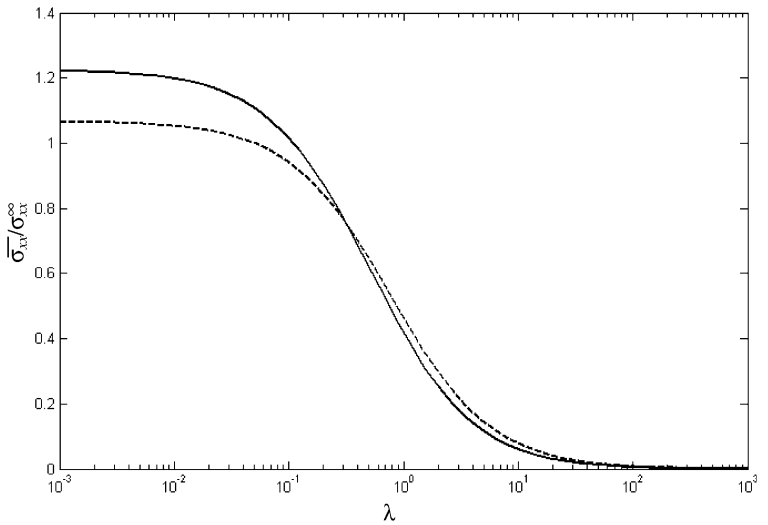

Fig. 4. Average stress $\overline{\sigma_{xx}}$ within the left inclusion as a function of the imperfect parameter λ when the remote stress is σ_{xx}^{∞}.

$\lambda = 0.27$, the peak traction occurs simultaneously at $\theta_2 = 0^0$ and $\theta_2 = 180^0$; when $\lambda > 0.27$ (the interphase layer is very compliant), the peak traction always occurs at $\theta_2 = 180^0$. No matter where the peak traction occurs, it is always a monotonic function of the imperfect parameter λ. The normal stress at the point $\theta_2 = 180°$, which is far away from the right circular inclusion, is very close to the result obtained by Eq. (57) for an isolated inclusion. This is due to the fact that only the stress field within the portion of the left inclusion, which is very proximate to the right inclusion, can be drastically perturbed by the neighboring right inclusion. Fig. 4 illustrates variations of average stress $\overline{\sigma_{xx}}$ within the left inclusion as a function of the imperfect parameter λ. The results when ignoring the perturbation due to the neighboring inclusion are also plotted as the dashed line. It is observed that (1) the average stress is a monotonic function of the imperfect parameter λ; and (2) the average stress will be higher than that of an isolated inclusion when the

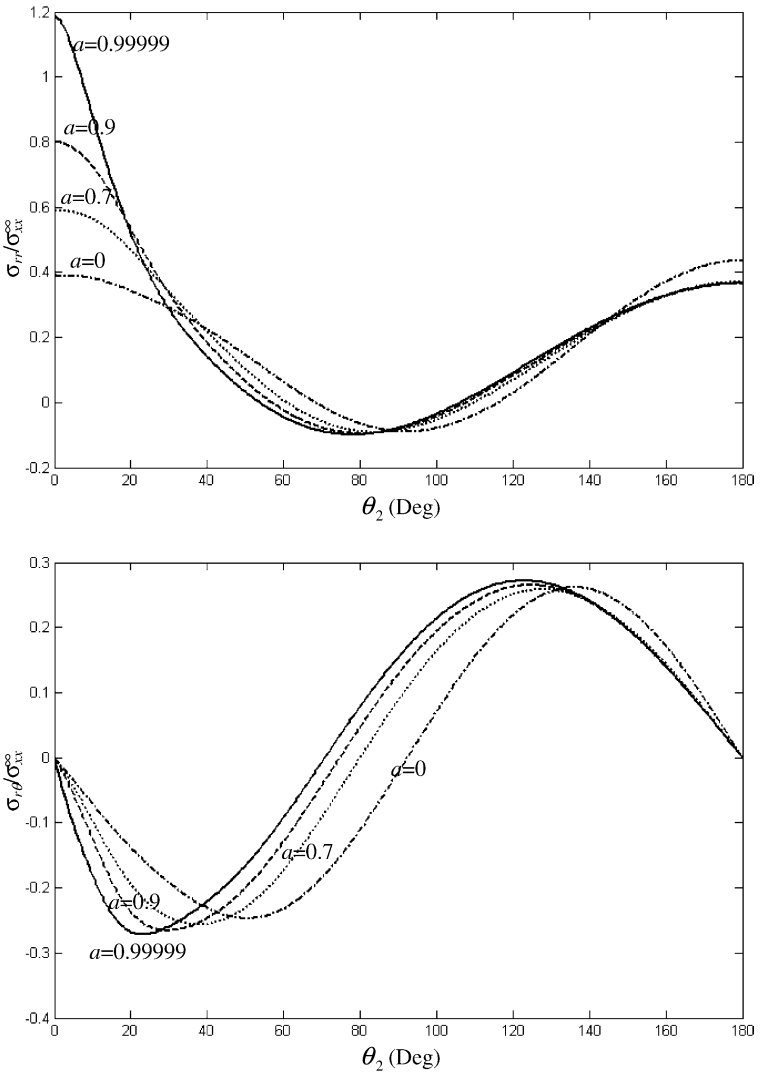

Fig. 5. Normal and tangential stresses along the left interface L_2 for different values of inhomogeneous parameter a when the remote stress is σ_{xx}^{∞} and $\lambda = 1$.

interfaces are relatively perfect ($\lambda < 0.27$), conversely the average stress will be lower than that of an isolated inclusion when the interfaces are relatively imperfect ($\lambda > 0.27$). It is of interest to notice that the uniform stress field within the left inclusion is nearly *unperturbed* by the right inclusion when $\lambda \approx 0.27$ even though the two inclusions are closed spaced.

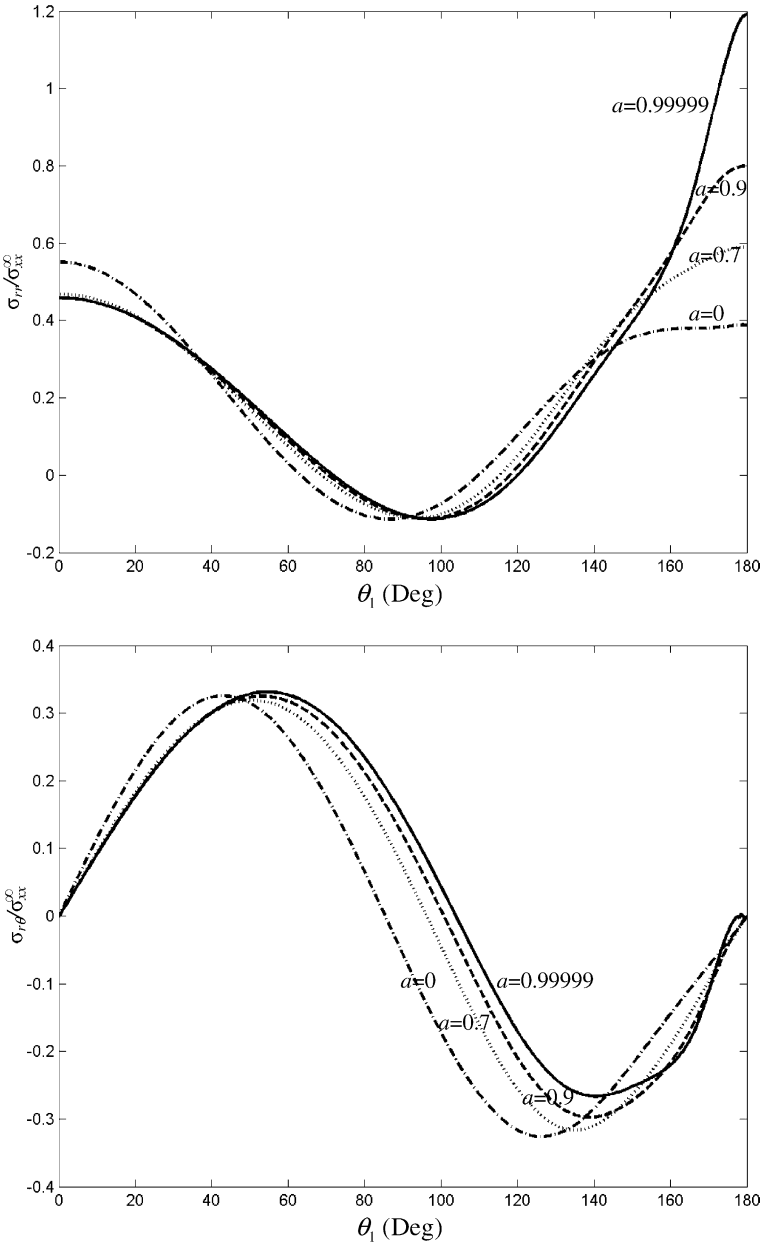

Fig. 6. Normal and tangential stresses along the right interface L_1 for different values of inhomogeneous parameter a when the remote stress is σ_{xx}^{∞} and $\lambda = 1$.

Next, we will consider inhomogeneously imperfect interfaces. Figs. 5 and 6 illustrate respectively the interface stresses along the left and right interfaces L_2 and L_1 for different a ($a = a_1 = -a_2$, $b_1 = b_2 = 0$) with $\lambda = 1$ ($\lambda = \lambda_1 = \lambda_2$). It is observed from Fig. 5 that when the degree of interface inhomogeneity increases, the maximum normal stress, which occurs at the most perfect part of the interfaces $\theta_2 = 0°$ and $\theta_1 = 180°$,

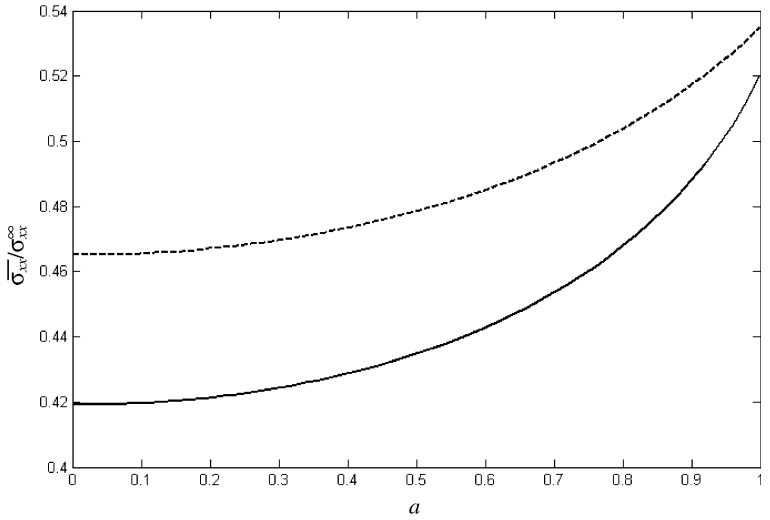

Fig. 7. Average stress $\overline{\sigma_{xx}}$ within the left inclusion as a function of the inhomogeneous parameter a when the remote stress is σ_{xx}^{∞} and $\lambda = 1$.

Table 1
The interfacial normal stress $\sigma_{rr}/\sigma_{xx}^{\infty}$ at $\theta_2 = 0°$ of the left interface L_2 when the shear moduli of the two inclusions are varied (the unit of $\mu_i (i = 1,3)$ is Gpa, and $\lambda = 1$, $a_1 = -a_2 = 0.99999$, $b_1 = b_2 = 0$)

μ_3	μ_1						
	74.22	100	200	400	800	10000	$+\infty$
34.9	1.1857	1.2694	1.4197	1.5136	1.5671	1.6209	1.6259
50	1.4294	1.5579	1.8026	1.9663	2.0638	2.1654	2.1748
75	1.7114	1.9044	2.2964	2.5795	2.7569	2.9498	2.9682
100	1.9076	2.1538	2.6767	3.0744	3.3330	3.6225	3.6506
125	2.0544	2.3438	2.9811	3.4851	3.8219	4.2078	4.2458
150	2.1664	2.4941	3.2314	3.8324	4.2428	4.7220	4.7697
175	2.2568	2.6163	3.4413	4.1303	4.6094	5.1773	5.2342
200	2.3310	2.7177	3.6200	4.3890	4.9316	5.5831	5.6489
250	2.4455	2.8765	3.9084	4.8160	5.4715	6.2748	6.3570
300	2.5299	2.9953	4.1313	5.1541	5.9061	6.8421	6.9386
400	2.6464	3.1616	4.4537	5.6559	6.5621	7.7156	7.8362
600	2.7765	3.3519	4.8380	6.2739	7.3881	8.8449	8.9996
800	2.8480	3.4577	5.0594	6.6397	7.8865	9.5417	9.7191
1000	2.8931	3.5252	5.2033	6.8815	8.2197	10.0141	10.2075
2000	2.9889	3.6701	5.5201	7.4248	8.9792	11.1100	11.3428
5000	3.0503	3.7641	5.7315	7.7957	9.5063	11.8863	12.1487
10000	3.0715	3.7967	5.8059	7.9280	9.6960	12.1688	12.4423
100000	3.0908	3.8267	5.8748	8.0511	9.8733	12.4343	12.7184
$+\infty$	3.0930	3.8301	5.8825	8.0650	9.8934	12.4645	12.7498

will also increase considerably. When $a \approx 1$, the maximum normal stress can get about $1.2\sigma_{xx}^{\infty}$ for both the two interfaces. Fig. 7 demonstrates variations of average stress $\overline{\sigma_{xx}}$ within the left inclusion as a function of the inhomogeneous parameter a with $\lambda = 1$. The results when ignoring the perturbation due to the neighboring inclusion are also plotted as the dashed line. The average stress is a monotonic function of the inhomogeneous parameter a. Also, the interaction between the two inclusions must be taken into account. In order to demonstrate the influence of the elastic properties of the two inclusions on the interfacial stresses, we show in Table 1 the dimensionless interfacial normal stress $\sigma_{rr}/\sigma_{xx}^{\infty}$ at the point $\theta_2 = 0°$ of the left interface L_2 when the shear moduli of the two inclusions are varied with $\lambda = 1$, $a_1 = -a_2 = 0.99999$, $b_1 = b_2 = 0$. It is observed that when the stiffness of the two inclusions increases, the magnitude of the normal stress will also increase. For the extreme case of two rigid inclusions, $\sigma_{rr} = 12.7498\sigma_{xx}^{\infty}$ at $\theta_2 = 0°$. Table 2 presents $\sigma_{rr}/\sigma_{xx}^{\infty}$ at the point $\theta_2 = 0°$ of the left interface L_2 for two rigid inclusions when the size and location of the right inclusion are varied with $\lambda = 1$, $a_1 = -a_2 = 0.99999$, $b_1 = b_2 = 0$. It is observed from Table 2 that the magnitude of the normal stress will increase rapidly when the right inclusion approaches the left inclusion. We guess that the normal stress becomes *singular* (infinite) when the two inclusions are just in contact with each other. This phenomenon is unique for two interacting inclusions with inhomogeneously imperfect interfaces. Our calculations demonstrate that the interfacial normal stress at $\theta_2 = 0°$ keeps *finite* for two rigid inclusions with homogeneously imperfect interfaces when $x_2 \to 1$.

Table 2
The interfacial normal stress $\sigma_{rr}/\sigma_{xx}^{\infty}$ at $\theta_2 = 0°$ of the left interface L_2 for two rigid inclusions when the size and location of the right inclusion are varied ($\lambda = 1$, $a_1 = -a_2 = 0.99999$, $b_1 = b_2 = 0$)

x_2	$(x_1 - x_2)/2$							
	0.25	0.5	1	2	2.5	3	4	5
1.0001	39.4600	74.6672	106.2926	118.6766	119.1730	116.2161	113.0220	108.8028
1.0005	21.6883	38.3043	54.1506	60.4655	60.5038	60.0938	58.7277	57.4520
1.001	15.4350	27.6189	39.0968	43.6572	43.6866	43.3872	42.5721	41.7335
1.005	7.0306	12.5787	17.8933	20.0210	20.0384	19.9075	19.1917	19.1275
1.01	4.8857	8.9197	12.7498	14.2905	14.3061	14.2211	13.8686	13.5361
1.05	2.2352	4.0025	5.7871	6.7102	6.6372	6.6021	6.4890	6.3658
1.1	1.5724	2.8533	4.1967	4.8129	4.8416	4.8240	4.7497	4.6647
1.5	1.3146	1.5409	2.0920	2.5509	2.6209	2.6513	2.6535	2.6285
2.0	1.4018	1.4420	1.7019	2.0980	2.1988	2.2621	2.3185	2.3315
3.0	1.4460	1.4449	1.5305	1.7830	1.8860	1.9678	2.0805	2.1470
4.0	1.4567	1.4531	1.4920	1.6543	1.7376	1.8123	1.9321	2.0174
5.0	1.4589	1.4557	1.4767	1.5865	1.6512	1.7137	1.8242	1.9160

Table 3
The value of normal stresses $\sigma_{rr}/\sigma_{xx}^{\infty}$ and their relative errors at the two points $\theta_2 = 0°$ and $\theta_2 = 5°$ for two rigid inclusions when different number of Laurent series is taken ($x_2 = 1.01$, $x_1 = 3.01$, $\lambda = 1$,$a_1 = -a_2 = 0.99999$, $b_1 = b_2 = 0$)

N	$\sigma_{rr}/\sigma_{xx}^{\infty}(\theta_2 = 0°)$	Relative error (%)	$\sigma_{rr}/\sigma_{xx}^{\infty}(\theta_2 = 5°)$	Relative error (%)
20	10.1758	20	4.5903	17.5
30	11.8487	7	3.3526	14
40	12.5022	1.9	3.9339	0.7
45	12.8506	0.8	3.8237	2
50	12.7065	0.3	3.9412	0.9
60	12.7557	0.05	3.8929	0.3
70	12.7607	0.08	3.9099	0.09
80	12.7565	0.05	3.9065	0.003
100	12.7498	0	3.9064	0

It is found that the present method is well suit to treat two extremely closely spaced inclusions. For example, for two inclusions of equal size ($x_1 - x_2 = 2$), we can get sufficiently accurate results for $x_2 = 1.01, 1.001, 1.0001, 1.00001, \ldots$ provided that the series be truncated at a sufficiently large number $N = 60, 200, 500, 1000, \ldots$, respectively. Before ending this subsection, we perform a convergence study to show how the number of terms in the Laurent series influences the solution. Table 3 presents the value of normal stresses $\sigma_{rr}/\sigma_{xx}^{\infty}$ and their relative errors at the two points $\theta_2 = 0°$ and $\theta_2 = 5°$ for two rigid inclusions embedded in an aluminum matrix when different number of Laurent series is taken with $x_2 = 1.01$,

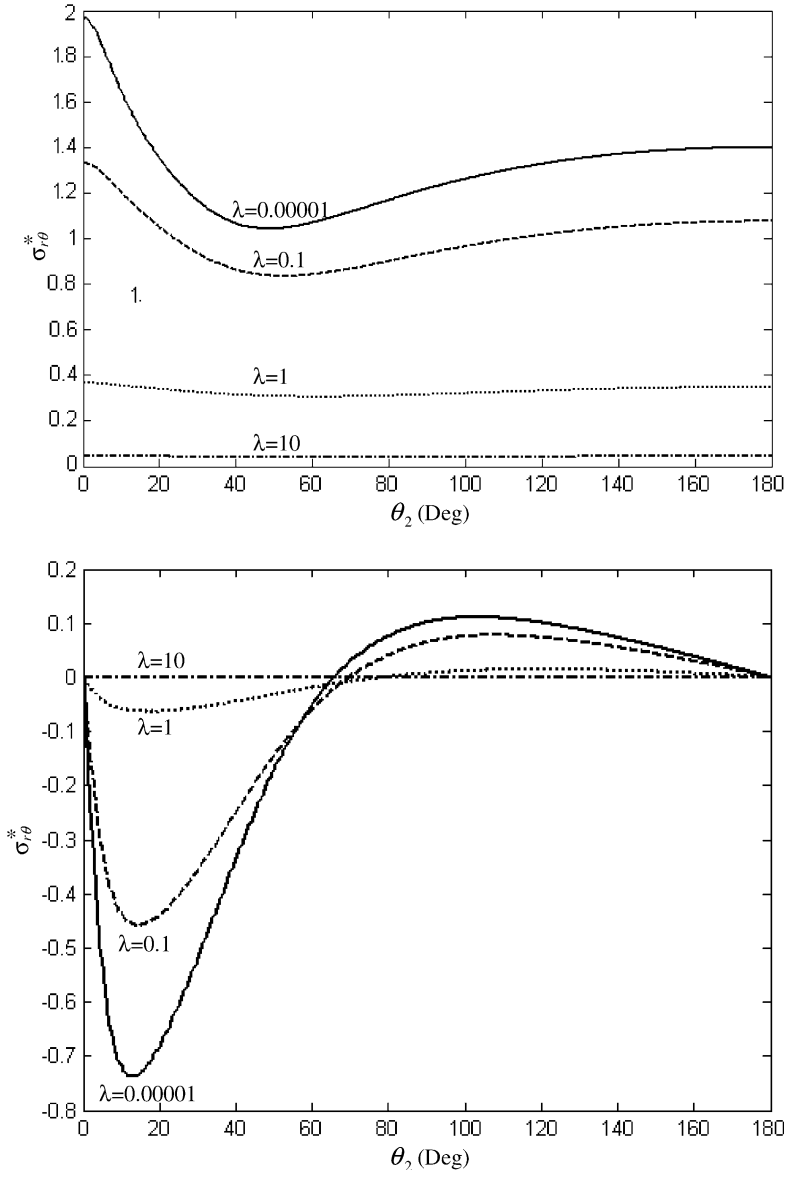

Fig. 8. Normal and tangential stresses along the left interface L_2 for different values of imperfect parameter λ under a uniform temperature change.

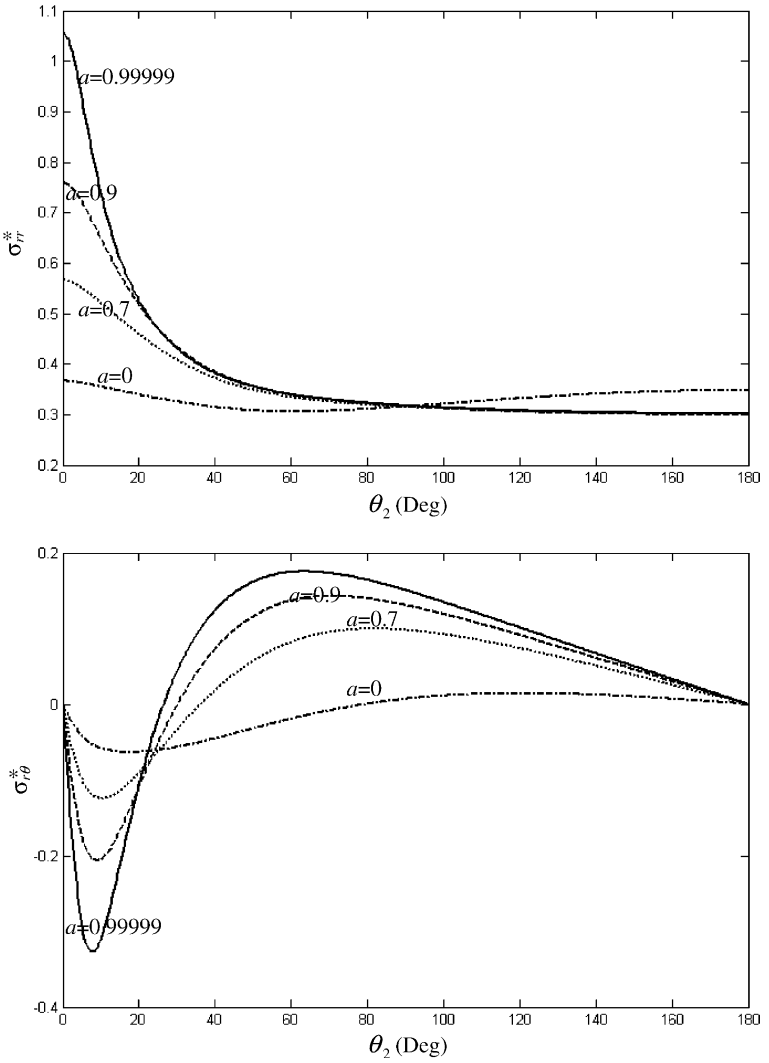

Fig. 9. Normal and tangential stresses along the left interface L_2 for different values of inhomogeneous parameter a under a uniform temperature change with $\lambda = 1$.

Table 4
The interfacial normal stress $\sigma^*_{rr} = -\frac{1+\kappa_2}{2\mu_2 \varepsilon^{**}_0}\sigma_{rr}$ at $\theta_2 = 0°$ of the left interface L_2 when $\lambda(\lambda = \lambda_1 = \lambda_1)$ and $a(a = a_1 = -a_2, b_1 = b_2 = 0)$ are varied

λ	a						
	0	0.4	0.7	0.8	0.9	0.99	0.99999
0.00001	1.9631	1.9631	1.9631	1.9631	1.9631	1.9631	1.9631
0.01	1.8681	1.8913	1.9097	1.9159	1.9220	1.9266	1.9268
0.1	1.3325	1.4303	1.5314	1.5740	1.6232	1.6756	1.6818
0.5	0.6122	0.7148	0.8568	0.9333	1.0437	1.2140	1.2449
1	0.3667	0.4451	0.5673	0.6409	0.7603	1.0010	1.0600
10	0.0444	0.0578	0.0840	0.1041	0.1473	0.3684	0.7249
100	0.0045	0.0060	0.0089	0.0112	0.0167	0.0561	0.5122

$x_1 = 3.01$, $\lambda = 1$, $a_1 = -a_2 = 0.99999$, $b_1 = b_2 = 0$. If the values for $N = 100$ are taken to be the exact results, then it is found that we can take $N = 40$ to get sufficiently accurate results with a relative error of less than 2%.

8.2. Uniform eigenstrains

In this subsection, we consider the case of a silicon matrix surrounding two aluminum inclusions of equal size. The material properties of the matrix and the inclusions are described by (Shen et al., 2001b)

$$\begin{aligned} &\nu_2 = 0.28, \quad \mu_2 = 74.22 \text{ Gpa}, \quad \alpha_2 = 2.5 \times 10^{-6}/^{\circ}\text{C} \\ &\nu_1 = \nu_3 = 0.33, \quad \mu_1 = \mu_3 = 23.31 \text{ Gpa}, \quad \alpha_1 = \alpha_3 = 25 \times 10^{-6}/^{\circ}\text{C}, \end{aligned}$$

where α denotes the coefficient of thermal expansion.

Also, we assume that $x_2 = 1.01, x_1 = 3.01$. For thermal stresses resulting from a uniform change (cooling) in temperature ΔT, the eigenstrains imposed on the two inclusions are given by

$$\begin{aligned} &\varepsilon_x^* = \varepsilon_y^* = \frac{(\alpha_1 - \alpha_2)\Delta T}{2}, \varepsilon_{xy}^* = 0, \\ &\varepsilon_x^{**} = \varepsilon_y^{**} = \frac{(\alpha_3 - \alpha_2)\Delta T}{2}, \varepsilon_{xy}^{**} = 0, \end{aligned} \tag{65}$$

First, we will consider homogeneous interfaces. In Fig. 8, the interfacial stress distribution ($\sigma_{rr}^* = -\frac{1+\kappa_2}{2\mu_2\varepsilon_x^{**}}\sigma_{rr}$, $\sigma_{r\theta}^* = -\frac{1+\kappa_2}{2\mu_2\varepsilon_x^{**}}\sigma_{r\theta}$) along the interface L_2 is plotted for different $\lambda (\lambda = \lambda_1 = \lambda_2)$. It is found that the normal stresses are always positive along the entire interface. This result is similar to that observed by Shen et al. (2001b) for an elliptical inclusion. Similar to the case of mechanical loading, the normal stress at the point $\theta_2 = 180^{\circ}$, which is far away from the right circular inclusion, is very close to the result obtained by Eq. (57) for an isolated inclusion. Due to the perturbation caused by the neighboring inclusion, the normal stresses are no longer uniform along the circular interface L_2 also the tangential stresses are non-trivial along the interface L_2 This phenomenon is especially true for those points which are very proximate to the right inclusion ($\theta_2 < 90^{\circ}$) and when the interfaces are relatively perfect (λ is very small). Also we observe that the introduction of compliant interface layers can effectively reduce interfacial stresses.

Next, we will consider inhomogeneously imperfect interfaces. Fig. 9 illustrates the interface stresses along the left interface L_2 for different a ($a = a_1 = -a_2, b_1 = b_2 = 0$) with $\lambda = 1$. It is observed that the non-uniformity of stresses is still significant when the degree of interfacial inhomogeneity is very serious, i.e., $a \to 1$. In this case, the non-uniformity of interfacial stresses mainly comes from interfacial inhomogeneity.

Table 4 presents the interfacial normal stress $\sigma_{rr}^* = -\frac{1+\kappa_2}{2\mu_2\varepsilon_x^{**}}\sigma_{rr}$ at the point $\theta_2 = 0^{\circ}$ of the left interface L_2 when the interface imperfection parameter λ ($\lambda = \lambda_1 = \lambda_1$) and the interface inhomogeneity parameter $a (a = a_1 = -a_2, b_1 = b_2 = 0)$ are varied. It is found that the interface inhomogeneity parameter a has a minimal influence on the normal stress when the interface is relatively perfect, i.e., $\lambda \to 0$, while the interface inhomogeneity parameter a exerts a significant influence on the normal stress when the interface is relatively imperfect, i.e., $\lambda \gg 1$.

9. Conclusions

This research analytically studies the plane elastic problem associated with two circular inclusions with circumferentially inhomogeneously imperfect interfaces embedded in an infinite matrix. It shall be mentioned that only the simplest inhomogeneous interfaces modeled by Eqs. (17) and (33) are adopted

in this research to simplify the analysis. Otherwise, the analysis will become more involved. Stresses due to uniaxial horizontal tension at infinity and resulting from a uniform change in temperature are calculated in the numerical examples. The following conclusions can be drawn from the numerical calculations:

1. The existence of the neighboring inclusion, the interface imperfection and the interface inhomogeneity can all significantly influence the stress field within and near each of the inclusions (along the interfaces). When the interfaces are relatively imperfect ($\lambda_1, \lambda_2 \gg 1$), the interface inhomogeneity plays a key role.
2. For homogeneously imperfect interfaces, the peak interfacial traction is a monotonic function of the interface imperfection parameter $\lambda(\lambda = \lambda_1 = \lambda_2)$ when the composite is subject to uniaxial horizontal tension at infinity. While the parameter λ can determine the location of the peak traction. Furthermore, the interface imperfection parameters λ_1 and λ_2 can be properly designed to achieve a very unique situation in which the uniform stress field within a certain inclusion is nearly unperturbed by the existence of the neighboring closely spaced inclusion.
3. The interfacial normal stress may become singular when two rigid inclusions with inhomogeneously imperfect interfaces are in contact with each other and when the composite is subject to uniaxial horizontal tension at infinity. This phenomenon is unique for inhomogeneously imperfect interfaces.
4. It is found that the normal stresses are always *positive* along the entire interfaces when the composite undergoes a uniform change in temperature. Consequently, the inhomogeneously imperfect interface model is particularly suitable to treat many interacting inclusions with uniform or non-uniform compliant interphase layers.
5. The present method is especially adaptive at investigating the extreme case where the two circular inclusions are nearly in contact with each other, i.e., $x_2 \to 1$ and where the degree of interface inhomogeneity is extremely serious, i.e., $a_i^2 + b_i^2 \to 1$, $(i = 1, 2)$.

One possible application of this research is that the imperfect interface parameters λ_1, λ_2 and the inhomogeneous interface parameters a_1, b_1, a_2, b_2 can be designed to minimize and control the interfacial stresses. Other loading conditions, such as an edge dislocation or a line force interacting with the two circular inclusions can also be treated similarly (the simpler problem of an edge dislocation or a line force interacting with two circular inclusions with *perfect* interfaces has been addressed by Wang and Shen (2001)).

Acknowledgement

The authors would like to thank referees for their very helpful comments, suggestions and useful references. X.W. is grateful to Prof. Y.P. Shen (Xi'an Jiaotong University) for fruitful discussions. This research was supported by the Excellent Young Teachers Program of the Ministry of Education of China, and the Shu-Guang Program of the City of Shanghai and the Key Project of Shanghai Fundamental Research (04JC14034).

References

Achenbach, J.D., Zhu, H., 1990. Effect of interphases on micro and macromechanical behavior of hexagonal-array fiber composites. J. Appl. Mech. ASME 57, 956–963.

Bigoni, D., Serkov, S.K., Valentini, M., Movchan, A.B., 1998. Asymptotic models of dilute composites with imperfectly bonded inclusions. Int. J. Solids Struct. 35, 3239–3258.

Cao, W.J., 1988. Conformal Mapping Theory and its Application. Shanghai Science and Technology Press, Shanghai (in Chinese).

Chen, T., 2001. Thermal conduction of a circular inclusion with variable interface parameter. Int. J. Solids Struct. 38, 3081–3097.

Dvorak, G., Zhang, J., 2001. Transformation field analysis of damage evolution in composite materials. J. Mech. Phys. Solids 49, 2517–2541.

England, A.H., 1971. Complex Variable Method in Elasticity. John Wiley and Sons, New York.
Gao, Z., 1995. A circular inclusion with imperfect interface: Eshelby's tensor and related problems. J. Appl. Mech. ASME 62, 860–866.
Gulrajani, S.N., Mukherjee, S., 1993. Sensitivities and optimal design of hexagonal array fiber composites with respect to interphase properties. Int. J. Solids Struct. 30, 2009–2026.
Kattis, M.A., Providas, E., 1998. Inplane deformation of a circular inhomogeneity with imperfect interface. Theor. Appl. Fract. Mech. 28, 213–222.
Kanaun, S.K., Jeulin, D., 2001. Elastic properties of hybrid composites by the effective field approach. J. Mech. Phys. Solids 49, 2339–2367.
Kouris, D., 1993. Stress concentration due to interaction between two imperfectly bonded fibers in a continuous fiber composite. J. Appl. Mech. ASME 60, 203–206.
Liu, Y., Ru, C.Q., Schiavone, P., Mioduchowski, A., 2001. New phenomena concerning the effect of imperfect bonding on radial matrix crack in fiber composites. Int. J. Eng. Sci. 39, 2033–2050.
Mogilevskaya, S.G., Crouch, S.L., 2002. A Galerkin boundary integral method for multiple circular elastic inclusions with homogeneously imperfect interfaces. Int. J. Solids Struct. 39, 4723–4746.
Mogilevskaya, S.G., Crouch, S.L., 2004. A Galerkin boundary integral method for multiple circular elastic inclusions with uniform interphase layers. Int. J. Solids Struct. 41, 1285–1311.
Muskhelishvili, N.I., 1953. Some Basic Problems of the Mathematical Theory of Elasticity. Noordhoff, Groningen.
Pan, L., Adams, D.O., Rizzo, F.J., 1998. Boundary element analysis for composite materials and a library of Green's functions. Comput. Struct. 66, 685–693.
Ru, C.Q., Schiavone, P., 1997. A circular inclusion with circumferentially inhomogeneous interface in antiplane shear. Proc. Roy. Soc. Lond. A 453, 2551–2572.
Ru, C.Q., 1998. A circular inclusion with circumferentially inhomogeneous sliding interface in plane elastostatics. J. Appl. Mech. ASME 65, 30–38.
Shen, H., Schiavone, P., Ru, C.Q., Mioduchowski, A., 2001a. Stress analysis of an elliptic inclusion with imperfect interface in plane elasticity. J. Elasticity 62, 25–46.
Shen, H., Schiavone, P., Ru, C.Q., Mioduchowski, A., 2001b. Interfacial thermal stress analysis of an elliptic inclusion with a compliant interface layer in plane elasticity. Int. J. Solids Struct. 38, 7587–7606.
Sudak, L.J., Ru, C.Q., Schiavone, P., Mioduchowski, A., 1999. A circular inclusion with inhomogeneously imperfect interface in plane elasticity. J. Elasticity 55, 19–41.
Tong, J., Nan, C.W., Fu, J., Guan, X., 2001. Effect of inclusion shape on the effective elastic moduli for composites with imperfect interface. Acta Mech. 146, 127–134.
Wang, X., Shen, Y.P., 2001. Green's functions for two circular inclusion problem in plane elastostatics. Acta Mech. Sin. 33, 639–654 (in Chinese).
Wang, X., Shen, Y.P., 2002. Two circular inclusions with inhomogeneous interfaces interacting with a circular Eshelby inclusion in anti-plane shear. Acta Mech. 158 (1-2), 67–84.
Zhong, Z., Meguid, S.A., 1997. On the elastic field of a spherical inhomogeneity with an imperfectly bonded interface. J. Elasticity 46, 91–117.